Multibeam, laser-imploded cylindrical plasmas

M. C. Richardson, R. Epstein, O. Barnouin, P. A. Jaanimagi,* R. Keck, H. G. Kim,
R. S. Marjoribanks, S. Noyes, J. M. Soures, and B. Yaakobi
Laboratory for Laser Energetics, University of Rochester, 250 East River Road, Rochester, New York 14623-1299
(Received 20 September 1985)

Four orthogonal line-focused 351-nm beams have been used to implode 2-mm-long, 100-μm-diam thin Al cylinders. The resulting linear, high-density, high-temperature plasma has characteristics suitable as an x-ray-laser medium.

I. INTRODUCTION

Many proposed x-ray-laser schemes incorporate a linear, high-density, high-temperature plasma generated by a cylindrically focused beam, or by multiple spherically focused beams from a high-intensity laser.[1] For the plasma to be optimum as an x-ray-laser medium, it should not only have density and temperature conditions appropriate for maximum population of the x-ray-laser ion states, but also have a geometric shape and uniformity of plasma conditions conducive to providing high x-ray gain along the axis of the plasma. Most experimental studies of collisionally excited or recombination x-ray laser schemes have so far used laser-produced plasmas created from solid targets. The characteristics of such plasmas produced by spherically focused laser beams have been investigated in great detail because of their application to laser fusion studies. Plasmas created by cylindrically focused laser beams have not been examined so thoroughly.[2] In some respects, plasmas produced from solid massive targets by short intense laser pulses are not ideal for x-ray-laser schemes. These plasmas have steep electron-density and temperature gradients across which ion-state populations are rapidly varying, making the conditions for x-ray gain highly transient. In general the plasma flow in these high-laser-intensity interactions is not stationary, and as a consequence regions of specific ion-state populations are not stationary with respect to an optical axis through the plasma, thereby limiting the time for which optimum gain conditions exist. Moreover, refraction of x-rays on the plasma density profile can contribute to an additional loss. These factors are compounded by the microscopic variations produced in the plasma profile by the small-scale variations in the intensity profile of most focused laser beams. These limitations can be alleviated with simple changes to the target design.

One approach to producing a more uniform plasma in which the effects of nonuniformities in the irradiating beam are smoothed out is to form the plasma from an exploding thin foil. There are several ways in which a thin foil can be exploded or decompressed in the early stages of its irradiation by a high-power laser pulse. It is well-known that the interaction of intense ($>10^{14}$ W cm^{-2}) short (<100 ps) long-wavelength ($\lambda \gtrsim 1$ μm) laser radiation with solid material is dominated by resonance absorption,[3] a process in which most of the absorbed energy is coupled through intense electromagnetic plasma waves to collisionless fast, or hot, electrons. In a thin-foil interaction, these hot electrons quickly explode the foil by electron energy deposition. Similar conditions may be achieved with intense short-wavelength radiation where rapid decompression of the foil results from shock and radiational heating.[4] Alternatively, targets fabricated of low-density material ($n < n_{\text{solid}}$) may be good candidates for x-ray-laser media, although the effects of self-induced whole-beam self-focusing may have to be taken into account.[5]

II. IMPLODING CYLINDRICAL TARGETS

We describe here two novel approaches to the development of a linear uniform medium suitable for x-ray gain conditions. Both these approaches depend upon the ability to uniformly compress cylindrical targets with multiple, line-focused laser beams. In these initial investigations, we have considered primarily Al cylinders for a number of reasons. The spectroscopy of Al is well-known,[6] and there are a number of transitions on which high gain can potentially be produced in a recombining plasma,[7,8] with or without enhanced plasma cooling.[8] With the limited energy currently available under line-focus conditions with OMEGA, we consider the implosion of cylinders of moderate Z, in which temperatures sufficiently high to ionize and excite the requisite energy levels can be generated (typically >400 eV). Thirdly, we chose Al because of its relative ease of fabrication in the form of free-standing, ultrathin-walled cylinders.

In this paper, we present some initial investigations of these ideas performed with four line-focused beams of the upconverted 351-nm OMEGA facility.[9] The four beams, each producing ≈ 50 J in ≈ 600 ps, were focused orthogonally onto the cylindrical target (Fig. 1) by an $f/3.7$ fused-silica lens combination comprising a high-power aspheric singlet lens and a close-coupled spherical cylindrical corrector plate, producing a line focus of length 1700 μm and width $\lesssim 50$ μm. Focused onto a target of ≈ 100-μm diameter, with the four beams tangentially overlapping the target, average irradiation intensities of $\sim 10^{14}$ W/cm^2 were produced. The four beams were coaligned with the aid of a solid reflective cylindrical surrogate target, from which fiducials were transposed to fixed high-resolution viewing systems for positioning the irradiated

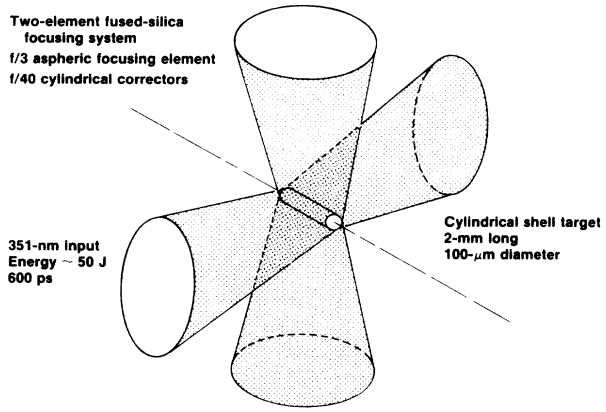

FIG. 1. Four-beam compression of cylindrical targets with orthogonal 351-nm line-focused beams of OMEGA.

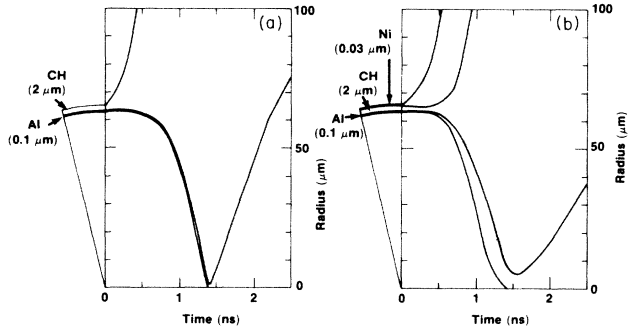

FIG. 3. Trajectories of material interfaces predicted by the one-dimensional hydrocode LILAC for the ablation target shown in Fig. 2(a). (a) shows the case for a low-Z center ablator, (b) shows the effect of adding a thin layer of high-Z material (Ni).

targets. Individual beams were aligned in position to an accuracy of $\approx 20\ \mu$m, and oriented parallel to one another to $\sim 10^{-2}$ rad. For the purpose of aligning the cylindrical plasma to the axis of diagnosing instrumentation, the axis of the cylindrical target could be set to an axis fixed to the enclosing vacuum chamber to an accuracy of 3×10^{-3} rad.

Two types of imploding targets were investigated, and compared to a solid Al cylinder target. These are illustrated in Fig. 2. The first, Fig. 2(a), comprised a 100-μm-diam CH cylindrical shell, 3—5 μm thick, the inside of which was coated with a 0.3-μm-thick layer of Al. The CH in this target serves as an ablator, its thickness being chosen to equal the ablation depth for an intensity of $\sim 10^{14}$ W/cm^{-2}.[10] Thus the Al layer is subjected to minimal heating until it stagnates at the center of the target. One-dimensional hydrodynamic simulations of this type of target with the Lagrangian code, LILAC (Fig. 3),[11] indicate that the Al reaches final density and temperature conditions of 4×10^{24} cm^{-3} and ≈ 300 eV, respectively, over a radial extent of $\lesssim 3\ \mu$m. Being ablatively driven by short-wavelength radiation, this target is sensitive to irradiation nonuniformities resulting from the use of only four beams. Were this final core density to be created it would be somewhat higher than the optimum for most soft-x-ray-laser schemes, and persists for only a short period of time. However, it is unlikely that the sharp central peak in density predicted by the one-dimensional hydrocode would, in reality, materialize. Some excursions from a uniform implosion would smooth the sharp density peak into the surrounding plasma. These conditions can in any case be modified by the addition of a thin ($\approx 0.015\ \mu$m) high-Z (Au) radiational source of preheat on the outside of the CH shell. The initial burst of x-ray emission from the Au shell penetrates the CH and preheats the Al before it is compressed. The resulting in-flight decompression of the Al leads to a reduced final core density. Although the temperature of the preheated target is reduced to ≈ 130 eV, the effect of the radiation from the outer layer is to increase (almost threefold) the duration over which the Al maintains a temperature in excess of 100 eV, to decrease the final core density by a factor ≈ 3 and to increase the spatial extent of the predicted central density peak to $\approx 10\ \mu$m.

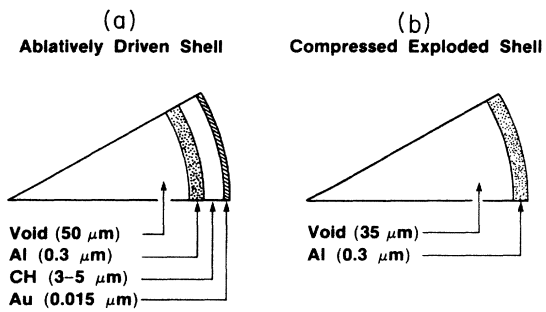

FIG. 2. Two types of cylindrical target designs investigated (a) a CH-coated metal cylinder, in which the CH acts as an ablator; (b) an ultrathin metal cylinder which explodes before being compressed.

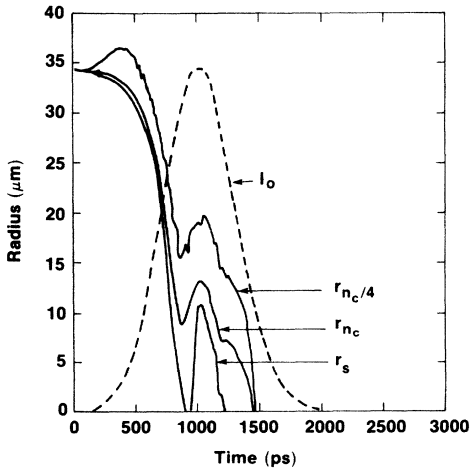

FIG. 4. One-dimensional simulation of the decompression and implosion of an ultrathin-walled metal (Al) cylindrical shell target.

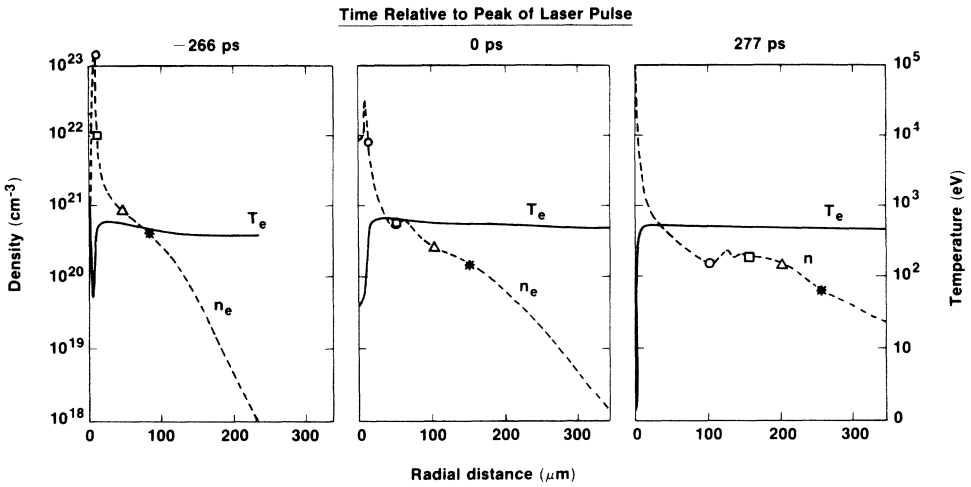

FIG. 5. Density and temperature profiles at different times following the implosion of a thin Al cylindrical shell of the type shown in Fig. 2(b).

The second type of cylindrical target is shown in Fig. 2(b). This consists of an ultrathin (0.3 μm) Al cylinder, ≈ 70 μm in diameter.[12] The target is fabricated by a novel method in which a solid cylinder of polystyrene is first overcoated with a thin layer of Al, and then leached away by chemical etching.[12] LILAC hydrocode simulations indicate that when irradiated, the thin Al cylindrical shell rapidly decompresses, reaching a mass-averaged density of $\approx 0.1 n_{\text{solid}}$, at a time ≈ 500 ps before the peak of the laser pulse (Fig. 4). The decompressed shell then rapidly implodes, producing at stagnation a small (≈ 30 μm diameter) high-density region in the center of the cylinder, surrounded by a lower density plateau (Fig. 5). A fairly large fraction (see Fig. 5) of the mass of the original shell is located in the high-density central region. In the post stagnation phase, this central high-density region unloads radially and aids in maintaining the long scale length of the electron density plateau. In Fig. 5, this phenomenon can be seen by following the outward flow of the Lagrangian cell marks with time. From Fig. 5, it can be seen that two regions of the plasma possess parameters suitable as an x-ray-laser medium. The narrow central region reaches electron densities higher than 10^{22} cm^{-3} over a radial extent of 10—20 μm with a temperature of several hundred electron volts. Although the code predicts a minimum in the electron temperature on axis, it is likely that in reality, the temperature in this region would be smoothed by small scale inhomogeneities. This high-density, high-temperature region persists for some time (several 100 ps) following the implosion, and therefore offers potentially an optimal medium for x-ray amplification. The underdense region of the plasma is maintained by flow of plasma from the dense core. Under the influence of continuing absorption during the remainder of the laser pulse, a long, radially expanding plateau of plasma of electron density larger than 10^{20} cm^{-3} is produced. Almost stationary in profile, and with an electron temperature approaching 1 keV, this plasma provides conditions generally considered optimum for collisional excitation or recombination pumped laser schemes.

III. EXPERIMENTAL INVESTIGATIONS

In order to test these concepts, exploratory experiments were made with cylindrical targets irradiated by four orthogonal, line-focused uv (351-nm) beams from the 24-beam OMEGA laser facility. The primary intent behind these investigations was to examine experimentally the target concepts described above with a view to determining the degree to which these implosions are one-dimensional (or geometrically uniform), and to what extent the code correctly predicts the plasma conditions.

Several experiments were performed with targets of the type illustrated in Fig. 2, and compared with uniformly irradiated solid Al cylindrical targets of the same diameter. An extensive array of diagnostics was deployed in these experiments (Fig. 6), including plasma calorimetry, x-ray photography, and time-integrated x-ray spectroscopy. Time-resolved x-ray measurements were made with two instruments, an x-ray transmission grating spectrograph coupled to a streak camera,[13] and an elliptical crystal spectrograph also coupled to a streak camera.[14]

Absorption was measured with an approximately isotropic array of 20 plasma calorimeters. These registered a uniform plasma blow-off distribution, with overall absorption of $\approx 50\%$ for the solid and ablatively driven

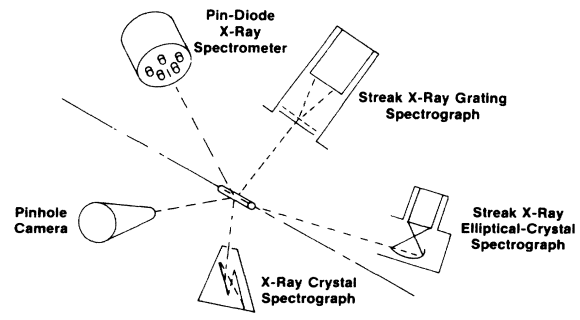

FIG. 6. Schematic of principal diagnostic systems deployed to characterize cylindrical plasma.

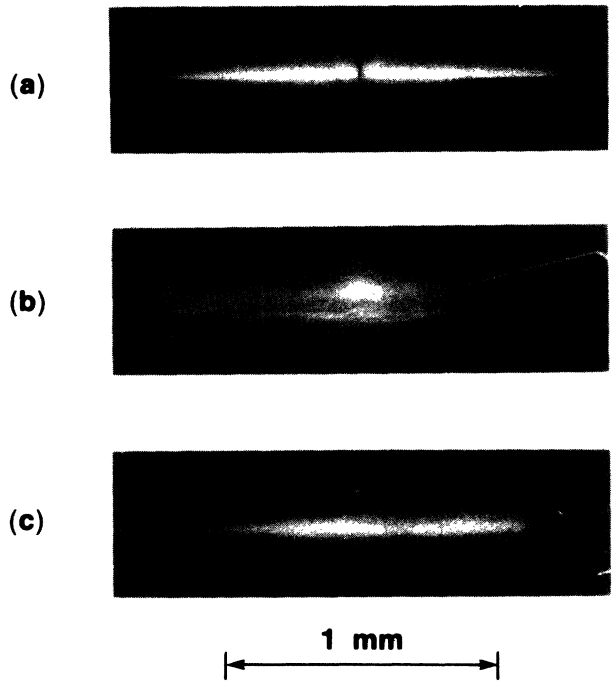

FIG. 7. X-ray pinhole photographs of cylindrical Al targets. (a) shows that of a solid Al target of 125 μm diameter, (b) an ablative target of Al type shown in Fig. 2(a), and (c) an ultrathin Al cylinder of $\approx$75 μm diameter.

cylinders, and typically $\approx$44% for the thin Al cylinders. These measured values of absorption are to be compared to those predicted by the LILAC hydrocode. These one-dimensional simulations assumed an $f/3.5$ cylindrical focusing geometry of beams focused 6 target radii beyond the target center. Account is taken for refraction of the beam in the plasma. The overall corona absorption predicted by LILAC was $\approx$57% for the thin Al cylindrical targets and $\approx$98% for the solid and ablatively driven targets. The latter value is comparable to that predicted and measured for solid spherical targets with 351-nm radiation at a similar intensity.[15] The somewhat lower measured values may be the result of a greater fraction of the laser energy being in the wings of the intensity distribution with cylindrical optics. Apart from x-ray photographic studies of the extent of the line focus, no optical measurements of the focal distribution have been made. In a previous study of line focus conditions,[2] an intensity distribution in the focal plane was measured in which about half of the energy resided in a broad, low-intensity plateau surrounding the main line-focused region.

X-ray image data of those types of targets irradiated is shown in Fig. 7. These were obtained with a pinhole x-ray camera (10-μm pinhole) in a 25-μm-thick Be filter, producing images in the 0.8—1.5-keV range. The x-ray image of the solid Al target [Fig. 7(a)] indicates qualitatively the apparent uniform illumination of the target in cylindrical geometry. Figure 7(b) shows the x-ray image of an ablatively driven Al shell. This particular target had an outer layer of Au; however, little difference in the x-ray emission from the target was observed if there was no Au layer. Weak x-ray emission from the core of the imploded shell can be observed. However, its uniformity along the 2-mm length of the target is poor, as is the linearity of the compressed core. Figure 7(c) shows the x-ray image of a compressed thin Al (0.3-μm) shell. The resulting x-ray emission is uniform and collinear with the original cylinder axis, and its radial extent ($\approx$25 μm diameter) is in good agreement with the LILAC predictions. Details of this image are shown in Fig. 8 which shows the

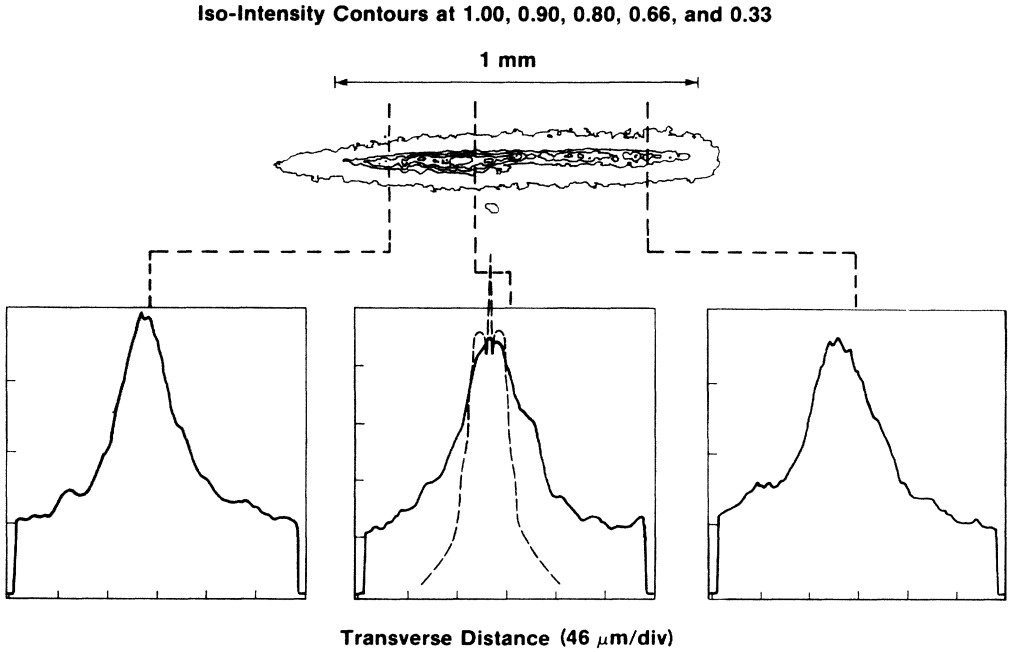

FIG. 8. Calibrated reduction of the x-ray image of the imploded ultrathin Al cylinder.

calibrated intensity of the x-ray emission, together with a LILAC prediction of the spatial extent of x-ray emission. Bright x-ray emission originates from a uniform linear core of ≈ 20 μm in radial extent. This is then surrounded by an annular region of 100 μm radial extent. Qualitatively this is similar to the predictions of the one-dimensional LILAC simulations shown in Fig. 5, which indicate the formation of a narrow high-density central compressed core unloading into a broader lower-density plateau.

The overall relative x-ray conversion was measured with the low-energy channels ($E < 3$ keV) of a 15-channel, K-edge-filter p-i-n diode—photomultiplier-scintillator x-ray continuum spectrometer. Assuming isotropy of x-ray emission, the total low-energy x-ray intensity from the CH ablative target, the Au-coated ablative target, the thin Al target, and the solid Al target were in the ratio 0.02:0.1:1.3:1.0.

Time-integrated x-ray spectra of Al emission were recorded with two planar crystal spectrographs situated coaxial and orthogonal to the axis of the cylindrical target axis. Each spectrograph employed a gypsum crystal ($2d = 15.15$ Å), and surveyed a spectral region of 6.6—8.0 Å. Spectra were recorded on Kodak RAR-2497 film developed according to the calibration of this film by Henke *et al.*[16] Figure 9 shows details of these spectra. The temperature of the emitting region was estimated from the ratio of the intensities of the Al Lyman α (7.173 Å) and the Al Heβ ($1s^2$-$1s3p$) at 6.635 Å. The latter transition is less sensitive to reabsorption than the Heα ($1s^2$-$1s2p$) transition. Assuming an optically thin plasma for the spectra observed orthogonally to the cylinder axis, and with the assumption of a collisional-radiative model,[17] a temperature of 600—700 eV is deduced.

Time-resolved x-ray spectroscopic studies of the x-ray emission from the line plasma were made with two streak spectrographs. These two instruments complemented one another in spectral resolution and range. The first of these instruments was a streak transmission grating spectrograph[13] which provided modest spectral resolution (1.5 Å) over a broad spectral range (1—30 Å), with a time resolution of ≈ 30 ps. This spectrograph observed x-ray emission was orthogonal to the cylinder axis and comprised a free-standing, 0.6-μm-thick, Au bar-grating with an interbar period of 3000 Å, in conjunction with a streak camera having a soft-x-ray-sensitive CsI photo-

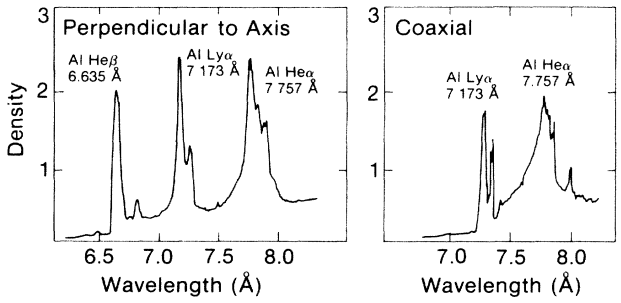

FIG. 9. Time-integrated x-ray spectra obtained collinear and orthogonal to the cylinder axis.

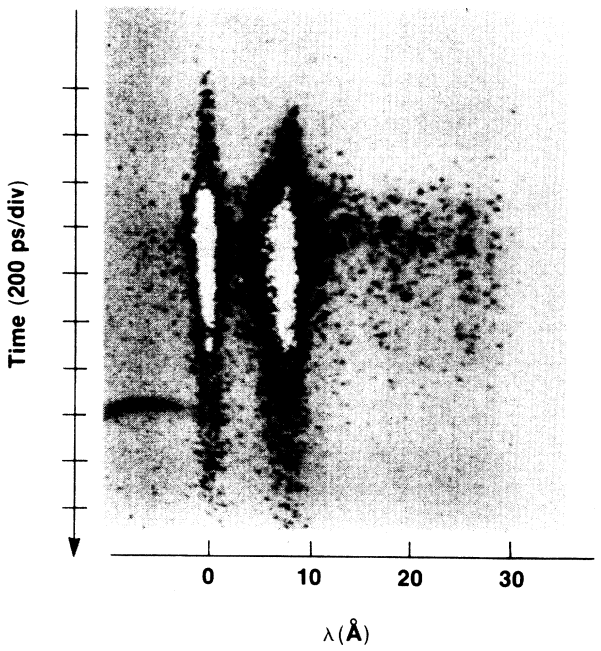

FIG. 10. Time-resolved soft-x-ray spectra from the streak transmission grating spectrograph. Data are those from an imploding ultrathin Al cylindrical target.

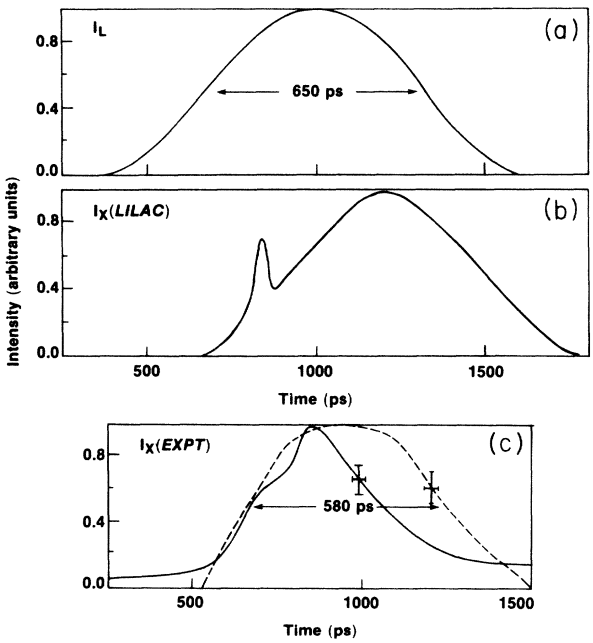

FIG. 11. Comparison of a time-resolved soft-x-ray data with predictions from LILAC. (b) shows the predicted x-ray emission in the range 1.5—2.2 keV compared to the duration of the laser pulse (a). (c) shows the measured shape of the x-ray emission in the 1.5—2.2-keV range (solid line) and the measured overall x-ray emission (dotted). No direct time relation was established between the x-ray emission and the laser pulse.

cathode (100 nm thick) deposited on a 70-nm-thick Formvar film overcoated with a 30-nm layer of Au. A typical time-resolved spectrogram of the compressed cylindrical plasma is shown in Fig. 10. The two-dimensional image recorded by the streak spectrograph was digitized and processed to remove image nonlinearities introduced by pin-cushion distortion in the streak camera image intensifier, and a nonlinear streak rate in the electron-optical deflection circuitry. The recorded emission is dispersed chiefly in the first order of the grating and shows the durations of the continuum emission and of the unresolved He-like and H-like Al resonance lines. Figure 11 shows the history of the x-ray emission as predicted by the one-dimensional hydrodynamic code post processed by a non-LTE (non—local-thermodynamic-equilibrium) model of ionization, together with representative experimental data recorded with the streak grating spectrograph. Figure 11(b) shows the predicted x-ray intensity in an x-ray window of 1.5—2.2 keV, approximately that region in which the resonance line emission from Al would fall on a time scale similar to that of the laser pulse, Fig. 11(a). A clear peak in the emission is obtained, corresponding to the time at which the decompressed shell stagnates at the center of the cylinder. This peak in x-ray emission is superimposed on top of a broad x-ray signal having a duration similar to the laser pulse. The second peak in x-ray emission observed in Fig. 11(b) coincides with the peak in the average temperature of the plasma, and also with the rebound compression in the compressed target, as indicated in Figs. 4 and 5. Typical temporal records of x-ray emission recorded from the streak grating spectrograph are shown in Fig. 11(c). The dotted trace shows the time history of all the x-ray radiation in the range 0.6—4.0 keV, and has a smoothly varying envelope of duration similar to the laser pulse. The solid curve shows the temporal shape of the emission in the range 1.5—2.2 keV, bracketing that region in which the resonance lines are emitted. In this trace, a sharp peak in the emission is observed, which could be interpreted as being due to the initial compression of the shell.

High-resolution time-resolved spectrograms of He-like and H-like Al resonance lines were recorded on a second streak spectrograph. This instrument provided high-resolution ($\lambda/\Delta\lambda \approx 600$) time-resolved spectra in the range 5—7 Å (1.77—2.48 keV) with a time resolution of 10 ps. This device consisted of a calibrated, elliptically curved PET (pentaerythritol) crystal combined with a second x-ray streak camera having a photocathode of CsI (120 nm thick) deposited onto a 12.7-μm Be substrate.[14] Typical

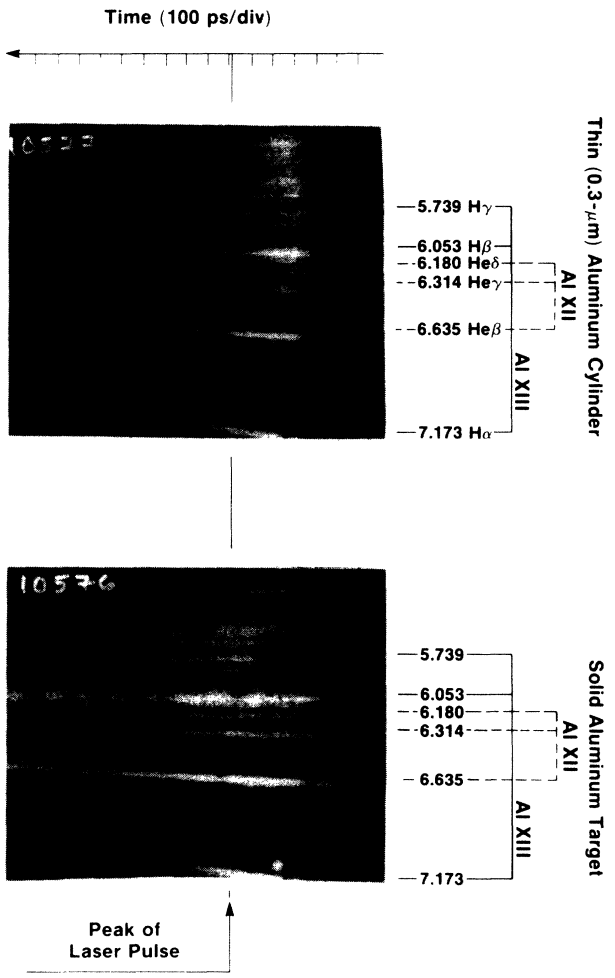

FIG. 12. Time-resolved x-ray spectra of Al resonance lines from ultrathin shell and solid targets.

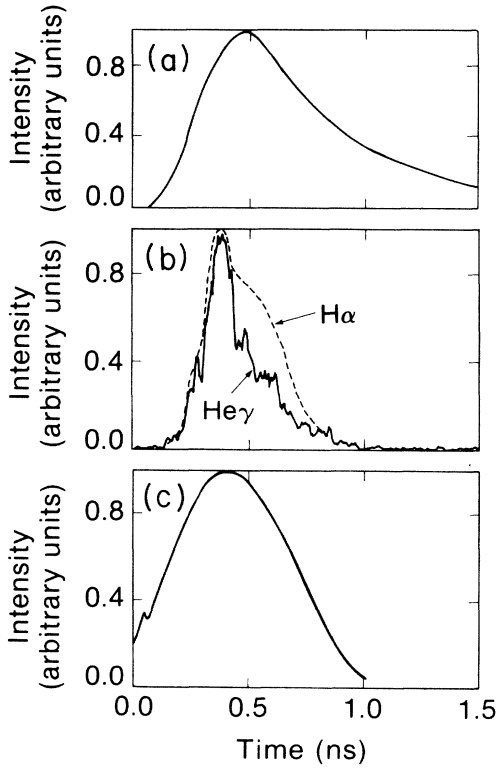

FIG. 13. Time profiles of the x-ray emission. (a) from the solid target; (b) from the Al shell target Al $1s$-$2p$ line (— — —), Al $1s^2$-$1s4p$ line (——); and (c) non-LTE simulation of the Al $1s$-$2p$ line intensity.

time-resolved spectra from this instrument are shown in Fig. 12. Figure 12(a) shows the spectra from a compressed cylindrical target, while that in Fig. 12(b) shows the duration of Al emission from the plasma off a solid Al rod target. Both the He-like and H-like lines can clearly be resolved, as well as the recombination emission at higher x-ray energies. The slight inward distortion in the streaked lines is due to an artifact in the streak tube. Figure 13 shows reduced data obtained from these streak spectrograms. Figure 13(a) shows the time duration of the integrated spectral emission in the 5—7.5 Å range recorded from the solid cylindrical target. The shape and duration of the emission is typical of the x-ray emission from the corona from a solid metallic target. In Fig. 13(b) is shown the time history of specific lines emanating from the compressed cylindrical target. The dotted line shows the duration of the Hα line whilst the solid line shows the time history of the Heγ line of Al. The overall duration of these individual lines is significantly shorter than the laser pulse and the x-ray emission which results from the coronal plasma produced off a solid target. The Hα line emission predicted by the non-LTE post processor is shown in Fig. 13(c) and is seen to be similar to the observed emission in duration and, to some extent, in shape. The peak in the simulated emission corresponds with the peak in the average temperature of the plasma. The differences in the detailed shapes of the observed and simulated emission histories may be related to effects causing the differences between the observed and simulated emission in Fig. 11, but the specific connection is not clear. The integration of the Heβ and Hβ lines and the comparison of their overall relative intensities provides an estimate of $\approx$500 eV for the averaged plasma temperature, in reasonable agreement with the predicted value.

IV. SUMMARY

This initial investigation of the plasma created by imploding cylindrical targets has provided some interesting data from which future studies can optimize the production of linear plasmas suitable as x-ray-laser media. From the present studies it is clear that thick ablatively driven cylindrical shells will only implode symmetrically under illumination conditions more uniform than used in these investigations. However, the submicron-thick metallic shells, which rapidly decompress upon irradiation, implode symmetrically to produce conditions which appear to be similar to these predicted by the one-dimensional code LILAC. Further studies are planned to examine in detail the production of specific atomic levels during shell implosions.

ACKNOWLEDGMENTS

The authors wish to acknowledge discussions with J. Delettrez, R. L. McCrory, S. Skupsky, and C. P. Verdon at the Laboratory for Laser Energetics; U. Feldman and J. Seely at the U.S. Naval Research Laboratory; and D. C. Matthews and M. Rosen at Lawrence Livermore National Laboratory. This work was supported by the U.S. Department of Energy Office of Inertial Fusion under agreement No. DE-FC08-85DP40200 and by the Laser Fusion Feasibility Project at the Laboratory for Laser Energetics which has the following sponsors: Empire State Electric Energy Research Corporation, General Electric Company, New York State Energy Research and Development Authority, Northeast Utilities Service Company, Ontario Hydro, Southern California Edison Company, The Standard Oil Company, and the University of Rochester.

*Permanent address: Lawrence Berkeley Laboratory, University of California, Berkeley, CA 94720.

[1]For a general review of the short-wavelength laser approach, see R. W. Waynant and R. C. Elton, Proc. IEEE **64**, 1058 (1976); F. V. Bunkin, V. I. Derzhiev, and S. I. Yakovlenko, Kvant. Elektron. (Moscow) **8**, 1621 (1981) [Sov. J. Quantum Electron. **11**, 981 (1981)].

[2]M. D. J. Burgess, R. Dragila, B. Luther-Davies, K. A. Nugent, A. J. Perry, G. J. Tallents, M. C. Richardson, and R. S. Craxton, Phys. Rev. A **32**, 2899 (1985).

[3]D. W. Forslund, J. M. Kindel, K. Lee, E. L. Lindman, and R. L. Morse, Phys. Rev. A **11**, 679 (1975); K. G. Estabrook, E. J. Valeo, and W. L. Kruer, Phys. Fluids **18**, 1151 (1975).

[4]Y. B. Zeldovich and Y. P. Raizer, *Physics of Shock Waves and High Temperature Hydrodynamic Phenomena* (Academic, New York, 1966), Vol. 1.

[5]H. Figueroa, C. Joshi, C. E. Clayton, H. Azecchi, H. A. Ebrahim, and K. A. Estabrook, in *Laser Interaction and Related Plasma Phenomena*, edited by G. Miley and H. Hora (Plenum, New York, 1984), Vol. 6, p. 527.

[6]R. L. Kelly and L. V. Palumbo, U.S. Naval Research Laboratory Report No. 7599, 1973 (unpublished).

[7]P. Jaegle, A. Carillon, P. Dhez, G. Jamelot, A. Sureau, and M. Cukier, Phys. Lett. **36a**, 167 (1971).

[8]Y. Conturie, B. Yaakobi, J. Delettrez, and J. M. Forsyth, in *Laser Techniques for Extreme Ultraviolet Spectroscopy (Boulder, 1982)*, edited by T. J. McIraith and R. R. Freeman (AIP, New York, 1982), p. 312.

[9]J. M. Soures, R. J. Hutchison, S. D. Jacobs, L. D. Lund, R. L. McCrory, and M. C. Richardson, *Proceedings of the Tenth Symposium on Fusion Engineering, Philadelphia* (IEEE, New York, 1983), p. 1392.

[10]B. Yaakobi, O. Barnouin, J. Delettrez, L. M. Goldman, R. Marjoribanks, R. L. McCrory, M. C. Richardson, and J. M. Soures, J. Appl. Phys. **57**, 4354 (1985).

[11]These simulations were run assuming ray tracing and collisional absorption of cylindrical irradiation, classical thermal transport with flux inhibition (f=0.045), SESAME equation-of-state tables [B. I. Bennett, J. D. Johnson, G. I. Kenley, and G. T. Rood, Los Alamos National Laboratory Report No. LA-7130, 1978 (unpublished)], and multigroup radiation transport using tabulated LTE opacities [W. F. Heubner, A. L. Merts, N. H. Magee, and M. F. Argo, Los Alamos National Laboratory Report No. LA-6760, 1977 (unpublished)], Rosseland-averaged over each photon-energy group. The non-LTE simulations involve re-solving the radiation problem for the n_i, T_e, information from a LILAC run using opacities and emissivities from atomic populations obtained from rate equations [R. Epstein, S. Skupsky, and J. Delettrez, J. Quant. Spectrosc. Radiat. Transfer (to be published)].

[12]H. Kim, S. Noyes, M. C. Richardson, and B. Yaakobi, J. Vac. Sci. Technol. (to be published).

[13]M. C. Richardson, R. S. Marjoribanks, S. A. Letzring, J. M. Forsyth, and D. M. Villeneuve, IEEE J. Quantum Electron. **QE-19**, 1861 (1983).

[14]B. L. Henke and P. A. Jaanimagi, Rev. Sci. Instrum. **56**, 1537 (1985).

[15]M. C. Richardson, R. S. Craxton, J. Delettrez, R. L. Keck, R. L. McCrory, W. Seka, and J. M. Soures, Phys. Rev. Lett. **54**, 1656 (1985).

[16]B. L. Henke, F. G. Fujiwara, M. A. Tester, C. H. Dittmore, and M. A. Palmer, J. Opt. Soc. Am. B **1**, 828 (1984).

[17]R. H. Huddlestone and S. L. Leonard, *Plasma Diagnostic Techniques* (Academic, New York, 1965), Chap. 5, p. 29.

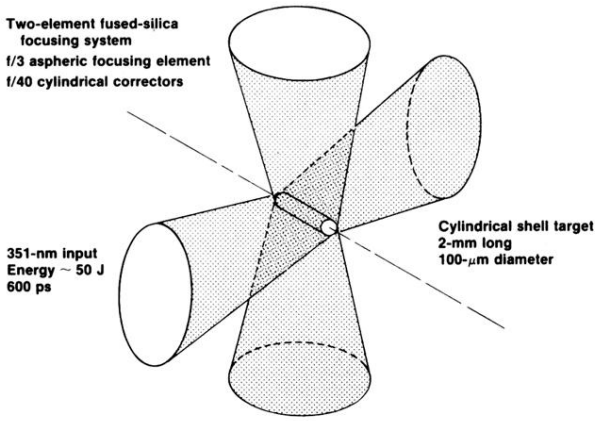

FIG. 1. Four-beam compression of cylindrical targets with orthogonal 351-nm line-focused beams of OMEGA.

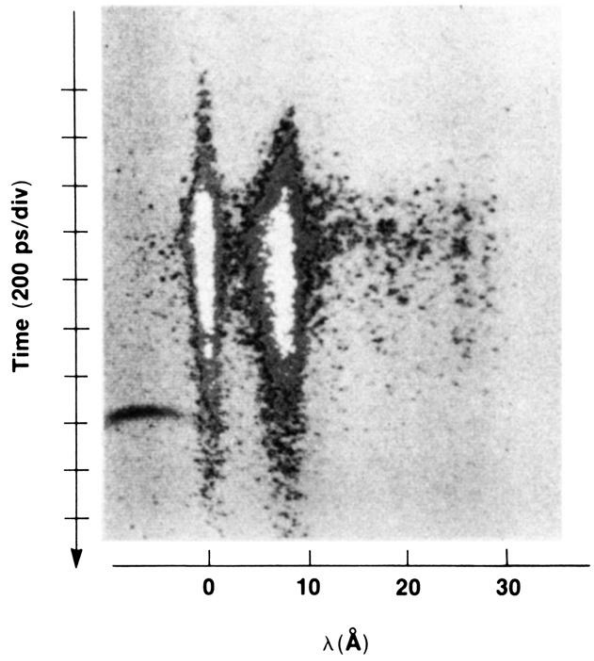

FIG. 10. Time-resolved soft-x-ray spectra from the streak transmission grating spectrograph. Data are those from an imploding ultrathin Al cylindrical target.

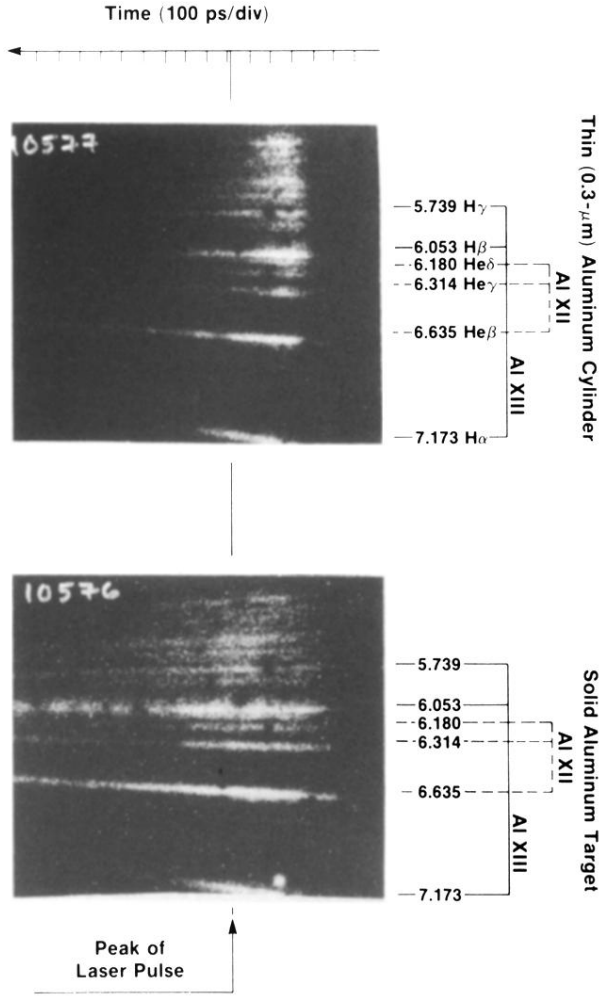

FIG. 12. Time-resolved x-ray spectra of Al resonance lines from ultrathin shell and solid targets.

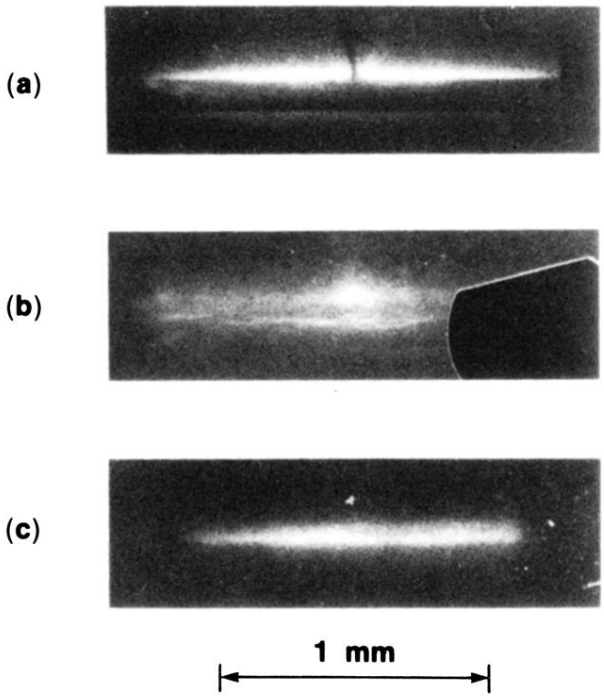

FIG. 7. X-ray pinhole photographs of cylindrical Al targets. (a) shows that of a solid Al target of 125 μm diameter, (b) an ablative target of Al type shown in Fig. 2(a), and (c) an ultrathin Al cylinder of ≈ 75 μm diameter.